Experimental and modeling investigation of CO_2 dissociation in Mars entry condition

Xin Lin', Lianzhong Chen, Jinlong Peng, Jinping Li, Fei Li, and Xilong Yu

Citation: AIP Conference Proceedings **1770**, 030121 (2016); doi: 10.1063/1.4964063
View online: http://dx.doi.org/10.1063/1.4964063
View Table of Contents: http://aip.scitation.org/toc/apc/1770/1
Published by the American Institute of Physics

Experimental and Modeling Investigation of CO_2 Dissociation in Mars Entry Condition

Xin Lin[1, 2, a)], Lianzhong Chen[1], Jinlong Peng[1], Jinping Li[2], Fei Li[2], Xilong Yu[2]

[1]*Beijing Key Laboratory of Arc Plasma Application Equipment, China Academy of Aerospace Aerodynamics, Beijing 100074, China.*
[2] *State Key Laboratory of High Temperature Gas Dynamics, Institute of Mechanics, Chinese Academy of Sciences, Beijing 100190, China.*

[a)]Corresponding author: linxin_bit@163.com

Abstract. Shock tube experiments are carried out to study the physical and chemical processes during a vehicle entry into the Mars atmosphere. The facility to establish a strong shock wave is a shock tube which is driven by combustion of hydrogen and oxygen. Measurements of rotational and vibrational temperature behind the shock wave are realized thanks to optical emission spectroscopy (OES). In parallel, tunable diode laser absorption spectroscopy (TDLAS) is utilized to diagnose one absorption line of CO near 2.33 μm. Combined with these temperature results using OES, CO concentration in the thermal equilibrium region is derived, which is 2.91×10^{17} cm^{-3}, corresponding to equilibrium temperature equals to 7000 ± 400 K. Moreover, a thermochemical code, based on Park's two-temperature theory, for studying chemical and physical processes is developed for Mars entry conditions. Some comparisons between experiments and calculations are presented. Such a two-temperature model fails to reproduce non-equilibrium temperatures and mole fractions but suitable for equilibrium temperature predictions.

INTRODUCTION

As we know, minimum-energy flight trajectories from Earth to Mars result in a Martian entry velocity of 5.8 km/s or much higher. Such a hypersonic velocity generates a strong shock wave in front of a space probe. The radiation emission is strongly dependent on the physical and chemical phenomena occurring in the shock layer. The dissociation of CO_2 is one of the most important reactions because it is the first chemical reaction to occur behind a shock wave. Therefore, an in-depth understanding of CO_2 dissociation occurring during the incubation period is extremely important for studying the physical and chemical phenomena in the shock layer and prediction of radiative heating environment for upcoming demanding missions [1].

Different groups from USA, Russia, Australia, Japan and Europe performed a number of shock-tube experiments for Mars entry using optical emission spectroscopy (OES) [2, 3]. OES is a well-known non-intrusive diagnostic technique that has been widely used for the absolute radiation and chemical reactions. Meanwhile, several thermodynamic models have also been established to rebuild these experiments and give an insight into the kinetic phenomena and non-equilibrium radiation occurring in the shock layer. However, because the experimental studies are not so exhaustive until now, many questions remain on chemical reaction modeling, especially on the dissociation of CO_2. All the simulation results revealed significant discrepancies when compared with shock-tube experiments.

According to the mentioned above, OES technology is not sufficient to validate relevant chemical models. Development of accurately quantitative diagnostic techniques for shock tube experiments is urgently needed. Tunable diode laser absorption spectroscopy (TDLAS) is a powerful tool to probe atoms and molecules non-intrusively in many areas [4]. Compared to other optical diagnostic applications, the ground state can be assessed.

International Conference on the Methods of Aerophysical Research (ICMAR 2016)
AIP Conf. Proc. 1770, 030121-1–030121-9; doi: 10.1063/1.4964063
Published by AIP Publishing. 978-0-7354-1428-0/$30.00

However, according to our knowledge, few studies have been conducted using TDLAS at such conditions for Mars atmospheric entry [5].

In this paper, gas temperature and CO concentration distribution behind a strong shock wave were simultaneously measured by an optical diagnostic system based on OES and TDLAS. Rotational and vibrational temperatures are obtained by analyzing the high temporal and spatial resolution experimental spectra of CN violet ($B^2\Sigma^+ \rightarrow X^2\Sigma^+$, $\Delta v = 0$) system. CO concentration distribution in the thermal equilibrium is determined by a TDLAS system near 2335.778 nm. Moreover, a thermochemical code, based on Park's two-temperature theory, for reproducing the experimental results (temperatures and species densities) in the shock layer is developed to study the mechanism of CO_2 dissociation for Mars atmosphere entry at the condition considered in this work.

MEASUREMENT TECHNIQUES

Optical Emission Spectroscopy (OES)

OES is a useful method in estimation of high-temperature gas behind a strong shock wave and is widely adopted as many literatures refer to [6]. Here, only a brief description is presented to define our notation.

The emission intensity is described as

$$I_{v'',J''}^{v',J'} = N_{v',J'} A_{v'',J''}^{v',J'} h\nu_{v'',J''}^{v',J'} \tag{1}$$

where (v', J') and (v'', J'') represent the vibrational and rotational quantum numbers in the upper level and lower lever, respectively, $N_{v',J'}$ is the population in the upper level (v', J') and obeys the Boltzmann distribution, $A_{v'',J''}^{v',J'}$ [s^{-1}] is the Einstein transition probability, h [J·s] is the Planck's constant and $\nu_{v'',J''}^{v',J'}$ [cm^{-1}] is the transition frequency.

The transition probability is expressed as

$$A_{v'',J''}^{v',J'} = \frac{64\pi \left(\nu_{v'',J''}^{v',J'}\right)^3 S_{J''}^{J'}}{3h(2J'+1)} q_{v',v''} R_e^2 \tag{2}$$

where $S_{J''}^{J'}$ is the Hönl-London factor, $q_{v',v''}$ is the Franck-Condon factor, and R_e^2 is the average value of the electronic transition moment. Assuming the Boltzmann distribution at each molecular state, fixing the value of v' and v'', and substituting Eq. (2) to Eq. (1), the emission intensity is described by

$$I_{v'',J''}^{v',J'} \propto \left(\nu_{v'',J''}^{v',J'}\right)^4 S_{J''}^{J'} \exp\left(-\frac{F(v',J')}{kT_r} - \frac{G(v')}{kT_v}\right) \tag{3}$$

where k [$J \cdot K^{-1}$] is Boltzmann constant, $F(v', J')$ [cm^{-1}] and $G(v')$ [cm^{-1}] are the rotational and vibrational energies, respectively. Based on the Eq. (3), the relative emission intensity depends on the rotational temperature and vibrational temperature. Generally, the routine method of rotational and vibrational temperature measurement is realized by iteratively comparison between a theoretical calculated spectrum and experimental spectrum.

Tunable Diode Laser Absorption Spectroscopy (TDLAS)

The fundamental theoretical principle of TDLAS is also well understood [7], and is reproduced here briefly. When a well collimated laser at frequency ν [cm^{-1}] enters a gas sample, a proportion of light is absorbed and the fractional transmission is described by the Beer-Lambert law expressed as

$$\left(\frac{I_t}{I_0}\right)_v = \exp(-\alpha_v) = \exp\left(-P_i \cdot S(T) \cdot \phi(v) \cdot L\right) \tag{4}$$

where I_0 and I_t are the incident and transmitted laser intensities, $(I_t/I_0)_v$ is the spectral transmittance, α_v is the spectral absorbance, P_i [atm] is the partial pressure of absorbing species (CO in this work), L [cm] is the optical path in the gas, practically the inner diameter of the shock tube, $S(T)$ [$cm^{-2}atm^{-1}$] and $\phi(v)$ [cm] are the line strength and line-shape function, respectively. The line strength $S(T)$ is a function of temperature as follows:

$$S(T) = S(T_0)\frac{Q(T_0)}{Q(T)}\left(\frac{T_0}{T}\right)\exp\left[-\left(\frac{hc}{k}\right)\left(E_1'' - E_2''\right)\left(\frac{1}{T} - \frac{1}{T_0}\right)\right]\frac{\left[1-\exp\left(-\frac{hcv_0}{kT}\right)\right]}{\left[1-\exp\left(-\frac{hcv_0}{kT_0}\right)\right]} \tag{5}$$

where h [J·s] is Planck's constant, k [$J \cdot K^{-1}$] is Boltzmann's constant, c [$cm \cdot s^{-1}$] is the speed of light, E'' [cm^{-1}] is the lower-state energy, v_0 [cm^{-1}] is the line-center frequency, T_0 [K] is the reference temperature (usually 296K), and $Q(T)$ is the partition function of the absorbing molecule CO. Since the line-shape function $\phi(v)$ is normalized to unity (defined as $\int \phi(v)dv \equiv 1$), the integrated absorbance A [cm^{-1}] can be calculated by taking the frequency integral of the absorption line-shape:

$$A = \int \alpha_v dv = P_{CO} \cdot S(T) \cdot L \tag{6}$$

In this study, rotational and vibrational temperatures are obtained through time gating OES diagnostics with nanosecond temporal resolution. Based on the ideal gas law, the CO concentration n_{co} can be deduced

$$n_{CO} = \frac{6.02\times10^{23} \cdot P_{CO}}{R \cdot T \cdot L}\left[\frac{101325 \cdot Pa}{1 \cdot atm}\frac{1 \cdot m^3}{100^3\, cm^3}\right] = \frac{6.1\times10^{22} \cdot A}{R \cdot T \cdot S(T) \cdot L}\left[cm^{-3}\right] \tag{7}$$

The transitions used in this study are shown in Tab. 1. These transitions are selected based on the spectroscopic parameters provided in the HITRAN 2008 database [8].

TABLE 1. Spectroscopic Line Parameters Used in the Current Study

Transitions	Wavelength λ, nm	Frequency v_0, cm^{-1}	Line Strength S@296K, $atm^{-1}cm^{-2}$	Low-State Energy E'', cm^{-1}
1	2335.544	4281.657	7.916×10^{-2}	57.670
2	2335.778	4281.228	1.483×10^{-7}	3378.954

CHEMICAL KINETIC CALCULATIONS

The kinetic code developed in our work is based on Park's two-temperature model (rotational/translational temperature T_r, vibrational/electronic temperature T_v). To simplify the calculations, a separate electron temperature T_e is not considered, instead T_e is assumed equal to vibrational temperature T_v because inelastic collisions between electrons and molecules are mainly responsible for vibrational excitation. Because of the lack of data, polyatomic molecules are taken into account as diatomic molecules.

The chemical kinetic model includes a total of 29 reactions and 14 chemical species: C, O, N, CO, C_2, N_2, CN, NO, O_2, CO_2, C^+, NO^+, NCO, e^-. A summary of chemical reactions and reactions rates is given in Tab. 2. As shown in the table, the chemical reaction rate is determined with an Arrhenius-type form as

$$k_f = CT_x^n \exp(-T_d / T_x) \tag{8}$$

where T_x is the temperature controlling the reaction and is assumed to be $\sqrt{T_r T_v}$ for all dissociation reactions, T_v for all reactions where an electron is a reactant, and T_r for the rest.

TABLE 2. Reaction rate coefficients for Martian atmosphere in the present model

	Reaction	*M*	T_x	C, $cm^3 mole^{-1} s^{-1}$	n	T_d	Source
	Dissociation						
1.	$C_2 + M \rightarrow C + C + M$	All	T_a	1.5×10^{16}	0.00	71600	Gokcen [9]
2.	$N_2 + M \rightarrow N + N + M$		T_a	7.0×10^{21}	-1.60	113,200	Park [10]
		C, O, N		3.0×10^{22}			Park [10]
		e^-		3.0×10^{24}			Gokcen [9]
3.	$O_2 + M \rightarrow O + O + M$		T_a	2.0×10^{21}	-1.50	59,750	Park [10]
		C, O, N		1.0×10^{22}			Park [10]
4.	$CN + M \rightarrow C + N + M$	All	T_a	2.53×10^{14}	0.00	71,000	Gokcen [9]
5.	$CO + M \rightarrow C + O + M$		T_a	2.3×10^{20}	-1.00	129,000	Park [10]
		C, O, N		3.4×10^{20}			Park [10]
6.	$NO + M \rightarrow N + O + M$		T_a	5.0×10^{15}	0.00	75,500	Park [10]
		N_2		1.45×10^{15}		74700	Park [10]
		CO_2		2.41×10^{15}			Park [10]
7.	$CO_2 + M \rightarrow CO + O + M$		T_a	6.9×10^{21}	-1.5	63275	Park [10]
		C, O, N		1.4×10^{22}			Park [10]
8.	$NCO + M \rightarrow CO + N + M$	All	T_a	6.3×10^{16}	-0.5	24000	Park [10]
	Neutral exchange						
9.	$N_2 + O \rightarrow NO + N$		T_r	6.4×10^{17}	-1.00	38370	Park [10]
10.	$NO + O \rightarrow O_2 + N$		T_r	8.4×10^{12}	0.00	19450	Park [10]
11.	$CO + C \rightarrow C_2 + O$		T_r	2.0×10^{17}	-1.00	58000	Park [10]
12.	$CO + O \rightarrow O_2 + C$		T_r	3.9×10^{13}	-0.18	69200	Park [10]
13.	$CO + N \rightarrow CN + O$		T_r	1.0×10^{14}	0.00	38600	Park [10]
14.	$N_2 + C \rightarrow CN + N$		T_r	5.24×10^{13}	0.00	22600	Gokcen[9]
15.	$CN + O \rightarrow NO + C$		T_r	1.6×10^{13}	0.10	14600	Park [10]
16.	$CN + C \rightarrow C_2 + N$		T_r	5.0×10^{13}	0.00	13000	Park [10]
17.	$CO + CO \rightarrow C + CO_2$		T_r	2.3×10^{9}	0.50	65710	Losev[11]
18.	$CO_2 + O \rightarrow CO + O_2$		T_r	2.1×10^{13}	0.00	27800	Park [10]
19.	$N_2 + C_2 \rightarrow CN + CN$		T_r	1.5×10^{13}	0.00	21000	Gokcen [9]
20.	$CO + NO \rightarrow NCO + O$		T_r	3.8×10^{17}	-0.873	51600	Park [10]
21.	$CN + O_2 \rightarrow NCO + O$		T_r	6.6×10^{12}	0.00	-200	Park [10]
22.	$CN + CO_2 \rightarrow NCO + CO$		T_r	4.0×10^{14}	0.00	19200	Park [10]
23.	$CN + NO \rightarrow NCO + N$		T_r	1.0×10^{14}	0.00	21200	Park [10]
24.	$CN + CO \rightarrow NCO + C$		T_r	1.5×10^{16}	-0.487	65800	Park [10]
25.	$CO + N \rightarrow NO + C$		T_r	2.9×10^{11}	0.50	53630	Losev [11]
26.	$NO + CO \rightarrow CO_2 + N$		T_r	4.6×10^{8}	0.50	12070	Losev [11]
	Charge exchange						
27.	$NO^+ + C \rightarrow NO + C^+$		T_r	1.0×10^{13}	0.00	23200	Park [10]
	Ionization						
28.	$O + N \rightarrow NO^+ + e^-$		T_r	8.8×10^{8}	1.00	31900	Park [10]
29.	$C + e^- \rightarrow C^+ + e^- + e^-$		T_v	3.9×10^{33}	-3.78	130700	Park [10]

EXPERIMENTAL APPARATUS

The experimental investigations are conducted in a hydrogen-oxygen combustion shock tube facility. Figure 1 gives an overview of the facility with useful dimensional details and the optical diagnostic system. The shock wave velocity is measured by three ion probes which are located on the shock tube. Experiments have been carried out in the mixture constituted of 70% CO_2 and 30% N_2. The mixture fills the test section with 100 Pa and the average shock velocity is equal to 7.09 ± 0.05 km/s.

Figure 1 also gives an overview of the optical diagnostic system, which consists of an OES system and a TDLAS system. Emission spectra are recorded using an Andor SR-500i spectrograph of focal length 500 mm. The spectrometer is equipped with an Andor DH-740 2048×512 pixels gated intensified CCD (ICCD) camera. By using a narrow line width diode laser (center wavelength: 777.19 nm, line width $\Delta\lambda < 0.001$ nm), the spectral resolution is measured and is equal to 0.154 nm with a Lorentz profile.

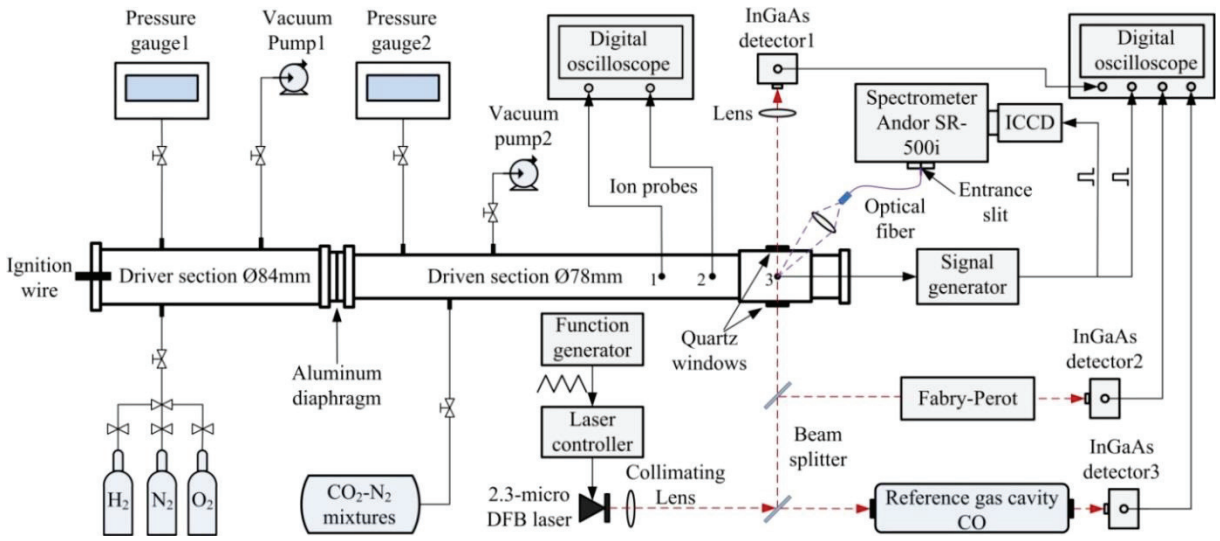

FIGURE 1. Schematic diagram of the experimental set-up of the shock tube and the optical experiments arrangement

For the TDLAS system, a DFB laser (Nanoplus GmbH) produces ~ 30 mW of stable output power near 2.33μm. Laser wavelength and intensity are controlled by a commercial controller (Thorlabs, Model: ITC-502). A scanned-wavelength direct absorption is used in present study. The injection current of the laser controller is modulated by a triangle ramp signal from a function generator (Tektronix, Model: AFG-3101) so that the lasing wavelength can probe the CO absorption transitions as shown in Tab. 1. The wavelength is modulated at a repetition rate of 50 kHz. The OES system and TDLAS system are triggered synchronously by an output signal of the No. 3 ion probe through a signal generator (Stanford Research System, Model: DG535) when the shock wave nears the location.

RESULTS AND DISCUSSIONS

Rotational and Vibrational Temperatures Determination

In our previous studies, the spectral structure of CN violet system has been investigated and a theoretical synthetic spectrum has been calculated based on our spectral resolution [12]. The rotational temperature can be determined by comparing the range (385 nm – 390 nm) of the CN violet system between the experimental and theoretical spectra. The vibrational structure of CN violet band system is apparent and the vibrational temperature is estimated by means of minimizing the error between the experimental and theoretical spectrum.

Figure 2 presents some comparisons of experimental spectra with theoretical synthetic spectra. As shown in Fig. 2a, the rotational temperature is significantly higher than the vibrational temperature at the beginning and the shock heated gas is in thermal non-equilibrium state obviously. In the quasi-equilibrium and equilibrium region, the

theoretical synthetic and experimental spectra match up very well and the optimum temperature fitting has been achieved.

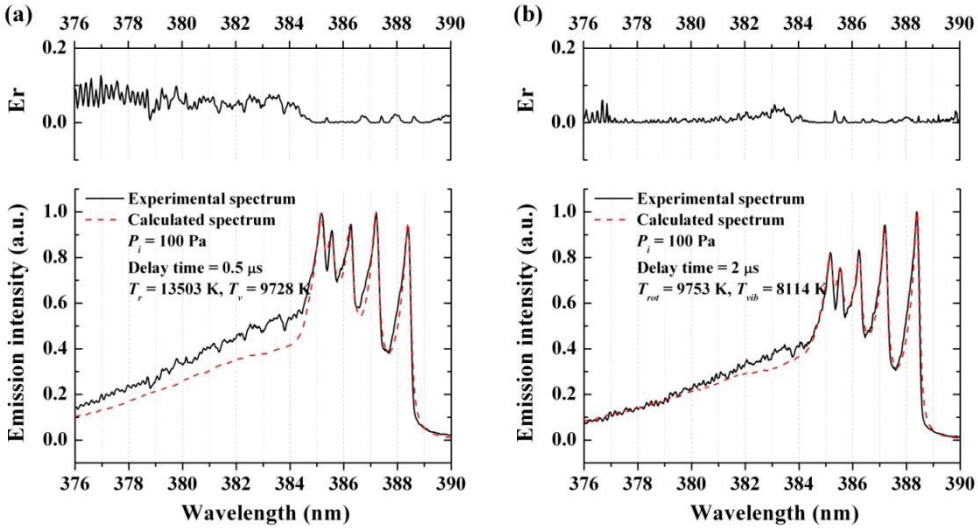

FIGURE 2. Experimental and theoretical synthetic spectra of CN violet system ($\Delta v = 0$) at different delay times (Experiment: p_i = 100 Pa, V_s = 7.09 ± 0.05 km/s. Composition: 70% CO_2 and 30% N_2)

CO Absorption Measurements behind the Strong Shock Wave

Figure 3 presents a typical absorption measurement signal behind a shock wave during one shot in the high pressure condition. In Fig. 3a, a sharp rising of the probe indicates the arrival of the incident shock at the location of the No. 3 probe. Figure 3b shows a direct-absorption scan using the TDLAS system, in which the laser intensity changes in response to an injection current ramp. Figure 4 shows an experimental absorption line-shape fitted with the Voigt profile, and the top portion shows the fitting residual.

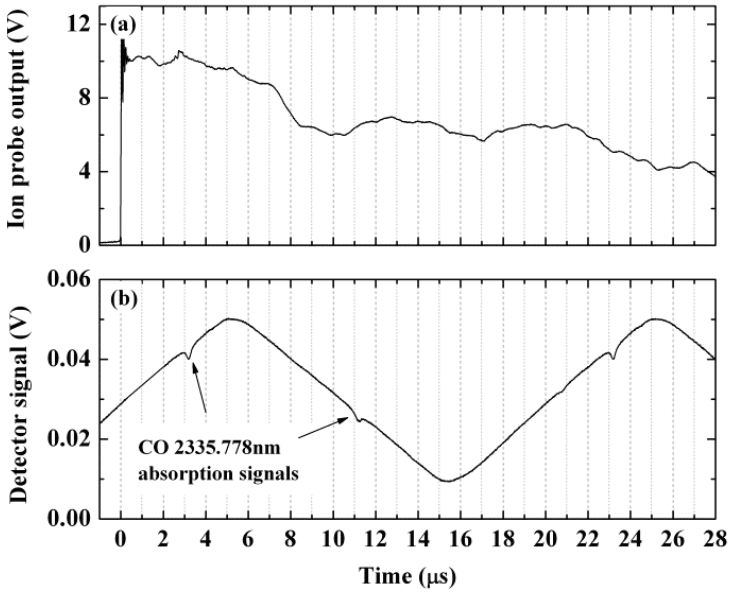

FIGURE 3. Raw experimental data behind a strong shock wave under the experimental conditions of P_i = 100 Pa and V_s = 7.08 km/s. (a) No. 3 ion probe output signal, (b) Detected absorbance signals for a direct absorption scan near 2335.778 nm.

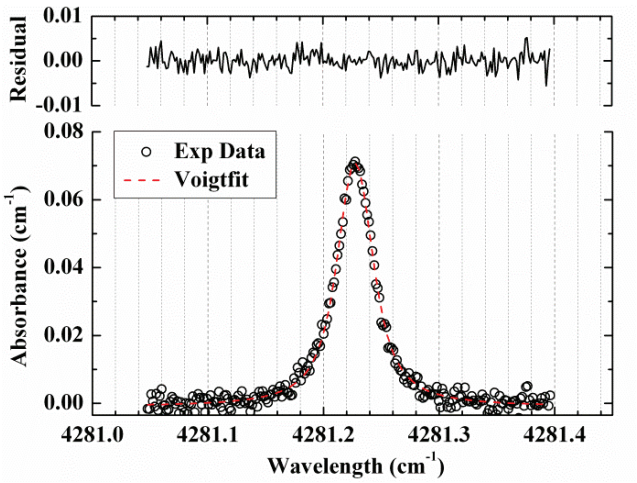

FIGURE 4. Single-scan absorption data for CO concentration measurement in a hydrogen-oxygen combustion driven shock tube with the CO transition near 2335.778 nm.

Figure 5 presents the evolutions of rotational and vibrational temperatures and integrated absorbance along the temperature distributions behind the shock waves using OES and TDLAS, respectively. For OES, each temperature point is deduced by the precise analysis of time gating spectral of CN violet system ($B^2\Sigma^+ \rightarrow X^2\Sigma^+$, $\Delta v = 0$ sequence). As shown in Fig. 5, both the rotational temperature and vibrational temperature rise very quickly with a relatively large uncertainty and the rise rate of rotational temperature is higher than the vibrational temperature. The non-equilibrium peak is evident from the profile. Afterwards, due to the high speed collision between gaseous particles, the thermal equilibrium between the rotational state and vibrational state is reached because of $T_r \approx T_v$. The experimental data reveals that the equilibrium temperature is found to be equal to 7000 ± 400 K after the delay time of 6 μs. For TDLAS, fluctuation of the integrated absorbance of CO is very slight in the thermal equilibrium region, and the variation tendency of the absorbance is consistent with the temperature results. It is considered that the chemical reactions in the high temperature gas have also achieved equilibrium after 6μs. Therefore, the deduced average CO concentration is 2.91×10^{17} cm^{-3} in the equilibrium region. In our studies, the integrated absorbance of CO in the non-equilibrium region can also be determined by TDLAS, however, they cannot be used to infer CO concentration because the CO number density in the non-equilibrium region do not follow the Boltzmann distribution at ground state and intense thermochemical reactions occurred in the non-equilibrium region lead many uncertain factors.

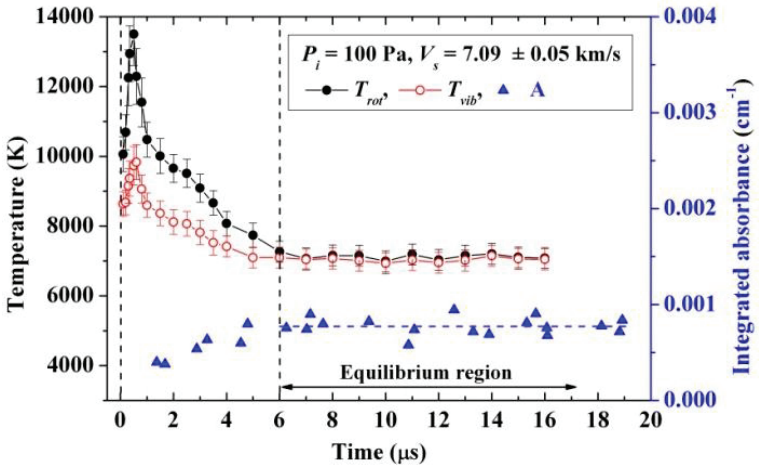

FIGURE 5. Evolution of the CO integrated absorbance and temperatures behind the shock wave under the experimental condition.

Comparisons with Chemical Kinetic Calculations

Figure 6 presents the comparisons of temperature and density profiles behind the shock wave between experimental results and the numerical calculations. Experiments and calculations are in rather good agreement for temperatures, especially when the rotational and vibrational temperatures are close. Anyway, in spite of selective successes, the two-temperature model cannot prove to be convenient to reproduce the non-equilibrium radiation. These computations also highlight that simple numerical models are not accurate enough to describe the non equilibrium of a gas behind a strong shock wave. This is a critical limitation of two-temperature models: they are not able to correctly deal with the kinetics of excited states. Some evolutions were recently proposed by taking into account precursor phenomena and using an improved translation–vibration exchange model.

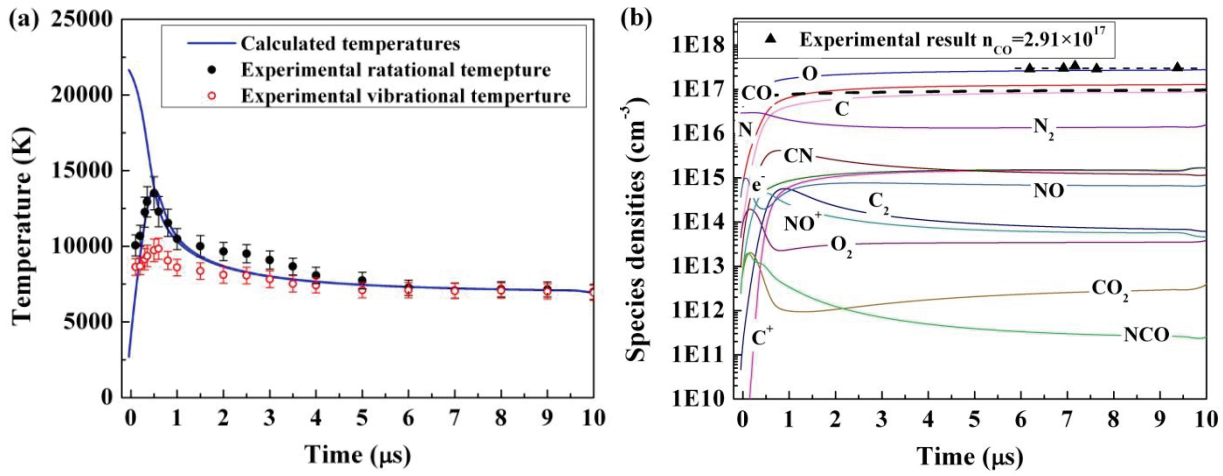

FIGURE 6. Comparison of the modeling results with measurements for our experimental condition (CO_2 70% - N_2 30%, p_i = 100 Pa, V_s = 7.09 km/s)

CONCLUSIONS

CO concentration distribution is diagnosed behind a strong shock wave simulating the Martian atmosphere entry processes by coupling OES and TDLAS. Experiments are carried out in a hydrogen–oxygen combustion driven shock tube. Time-resolved emission spectroscopy allows an analyzing time evolution of CN violet system ($B^2\Sigma^+ \rightarrow X^2\Sigma^+$, $\Delta v = 0$ sequence) and rotational and vibrational temperatures from the shock to the thermochemical equilibrium. Meanwhile, a CO absorption line near 2335.778 nm is selected for detecting the CO concentration and is simultaneously monitored and calibrated through a room temperature reference cavity and a Fabry-Perot interferometer. Scanned-wavelength direct absorption mode is utilized in our study.

Moreover, a thermochemical code, based on Park's two-temperature theory, for studying chemical and physical processes is developed for Mars entry conditions. Some comparisons between experiments and calculations are presented. Such a two-temperature model fails to reproduce non-equilibrium temperatures and mole fractions but suitable for equilibrium temperature predictions.

REFERENCES

1. T. Marynowski, S. Löhle, and S. Fasoulas, Journal of Thermophysics and Heat Transfer **28(3)**, 394-400 (2014).
2. V. A. Gorelov, M. K. Gladyshev, A. Yu. Kireev, et al., Journal of Applied Mechanics and Technical Physics **41(6)**, 970-976 (2000).
3. C. Rond, A. Bouber, P. Boubert, et al., Chemical Physics **354**, 16-26 (2008).
4. X. Chao, J. B. Jeffries and R. K. Hanson, Measurement Science and Technology **20**, 115-201 (2009).
5. X. Lin, X. L. Yu, F. Li, et al., Applied Physics B: Lasers and Optics **110**, 401-409 (2012).
6. C. O. Laux, *Optical Dignostics and Radiative Emission of Air Plasmas* (Stanford University, 1993).

7. I. A. Schultz, C. S. Goldenstein, R. M. Spearrin, et al., Journal of Propulsion and Power **30(6)**, 1595-1604 (2014).
8. L. S. Rothman, I. E. Gordon, A. Barbe, et al., Journal of Quantitative Spectroscopy & Radiative Transfer **110**, 533-572 (2009).
9. T. Gökçen, Journal of Thermophysics and Heat Transfer **21(1)**, 9-18 (2007).
10. C. Park, J. T. Howe, R. L. Jaffe, et al., Journal of Thermophysics and Heat Transfer **8(1)**, 9-23 (1994).
11. S.A. Losev and G.G. Chernyi, "Development of Thermal Protection System for Interplanetary Flight", International Science andTechnology Center, Moscow State Univ., Rept. N 036-96, Moscow, 1999.
12. X. Lin, X. L. Yu, F. Li, et al, Acta Mechanica Sinica **28(5)**, 1296-1302 (2012).